Reverse-correlation analysis of navigation dynamics in *Drosophila* larva using optogenetics

Luis Hernandez-Nunez[1, 2], Jonas Belina[3], Mason Klein[2], Guangwei Si[2], Lindsey Claus[2], John R. Carlson[3], and Aravinthan D.T. Samuel[2]

1. Center for Systems Biology, Harvard University, Cambridge, MA 02138
2. Department of Physics and Center for Brain Science, Harvard University, Cambridge, MA 02138.
3. Department of Molecular, Cellular, and Developmental Biology, Yale University, New Haven CT 06511

To Whom Correspondence Should be Addressed:
Aravinthan Samuel
17 Oxford Street
Cambridge, MA 02138
Email: samuel@physics.harvard.edu

Phone: 617-384-9435

Abstract

Neural circuits for behavior transform sensory inputs into motor outputs in patterns with strategic value. Determining how neurons along a sensorimotor circuit contribute to this transformation is central to understanding behavior. To do this, a quantitative framework to describe behavioral dynamics is needed. Here, we built a high-throughput optogenetic system for *Drosophila* larva to quantify the sensorimotor transformations underlying navigational behavior. We express CsChrimson, a red-shifted variant of Channelrhodopsin, in specific chemosensory neurons, and expose large numbers of freely moving animals to random optogenetic activation patterns. We quantify their behavioral responses and use reverse correlation analysis to uncover the linear and static nonlinear components of navigation dynamics as functions of optogenetic activation patterns of specific sensory neurons. We find that linear-nonlinear (LN) models accurately predict navigational decision-making for different optogenetic activation waveforms. We use our method to establish the valence and dynamics of navigation driven by optogenetic activation of different combinations of bitter sensing gustatory neurons. Our method captures the dynamics of optogenetically-induced behavior in compact, quantitative transformations that can be used to characterize circuits for sensorimotor processing and their contribution to navigational decision-making.

Introduction

To successfully navigate their environments, animals transform sensory inputs into motor outputs in patterns that strategically orient themselves towards improving conditions. The navigational strategies of insect larvae represent a long-standing paradigm for studying the mechanisms of animal orientation (1, 2). The small size and simple nervous system of the *Drosophila* larva, combined with its powerful genetic toolbox and recent advances in optical neurophysiology and anatomical reconstruction of circuit structure and connectivity, opens the possibility of understanding the neural encoding of animal navigation from sensory inputs to motor outputs without gaps (3). To accomplish this a quantitative framework to describe navigation decision-making is needed. Such a framework can then be used to dissect the function of the neurons and circuits in charge of processing sensory information.

Drosophila larva navigation involves the regulation of transitions between two basic motor states, runs during which the animal moves forward using rhythmic peristaltic waves and turns during which the larva sweeps its head back and forth until it selects the direction of a new run (4-6) (Fig 1A). Attractive and repulsive responses can be estimated by the tendency of the larva to aggregate near or avoid an environmental stimulus (7). Attractive and repulsive responses can also be observed in the movement patterns of individual larvae (4, 8, 9). When the larva encounters improving conditions over time, it lowers the likelihood of ending each run with a turn, thereby lengthening runs in favorable directions. When the larva encounters improving conditions during each head sweep of a turn, it increases the likelihood of starting a new run, thereby starting more runs in favorable directions. Thus, subjecting the larva to an attractant tends to suppress transitions from runs to turns and stimulate transitions from turns to runs; subjecting the larva to a repellant has the opposite effects.

Much progress has been made in understanding the molecular and cellular organization of the chemosensory system of the *Drosophila* larva, but how specific chemosensory neurons relay information to guide navigational movements remains poorly understood. (7, 10-12). One challenge of studying chemotaxis is that it is difficult to provide sensory input to behaving animals with the flexibility, receptor-specificity, and precision needed to build computational models of chemosensory-guided navigation. The recent development of a red-shifted version of Channelrhodopsin, CsChrimson, which is activated at wavelengths that are invisible to the larva's phototaxis system, now allows us to specifically manipulate the activity of neurons in behaving animals with reliability and reproducibility (13).

Here, we sought a mathematical characterization of the navigation dynamics evoked by optogenetic activation of different sets of neurons. We focus on the navigation driven by chemosensory inputs. Although the organization of the chemosensory periphery is well defined, the quantitative mapping from sensory activity to behavioral dynamics has not yet been determined. To do this, we engineered a high throughput experimental setup capable of recording the run and turn movements of freely moving larvae subjected to defined optogenetic activation of selected chemosensory neurons. By measuring large

numbers of animals responding to defined random patterns of optogenetic stimulation, we were able to collect enough data to use reverse-correlation analysis to connect optogenetic activation patterns of sensory neurons with motor patterns (14). We used this information to build linear-nonlinear (LN) models that accurately predict behavioral dynamics in response to diverse patterns of optogenetic activation of sensory neurons (15).

We used our method to study how the optogenetic activation of olfactory receptor neurons (ORNs) and different sets of gustatory receptor neurons (GRNs) map to navigational movements. Analysis of gustatory neurons allowed us to investigate the navigational responses evoked by individual GRNs and their combinations. We find that compact LN models that connect optogenetic activation to behavioral responses are nonetheless sufficient to describe or predict navigational behavior, and should facilitate future studies to elucidate the circuit mechanisms that shape sensorimotor transformations.

Results

Reverse-correlation analysis of navigation dynamics

We can characterize the navigation strategy of the *Drosophila* larva by identifying the mathematical functions that describe transitions between two basic motor states: running and turning (Fig 1A). We sought these functions ($f_{r\to t}$, $f_{t\to r}$) for defined patterns of chemosensory stimulation delivered via optogenetics. We used transgenic animals that express the red-shifted Channelrhodopsin CsChrimson in selected olfactory and gustatory neurons using the UAS-Gal4 system (16). In our setup, we followed the movements of large numbers of late second instar larvae navigating the surface of a 22 cm x 22 cm agar plate under dark-field illumination provided by infrared LEDs (Fig 1B). The entire plate was subjected to spatially uniform optogenetic illumination from above using a matrix of 625 nm red LEDs, a wavelength chosen to activate CsChrimson while invisible to the larva's photosensory system (13, 17). We tuned our light intensity (1.9 W/m^2) to a level where negligible behavioral response is detected in wild type animals crossed with *UAS-CsChrimson* fed with 0.5mM all-trans-retinal. We made sure that this light intensity is strong enough to activate CsChrimson by testing it with a well-studied motor neuron line (Fig 1-figure Supplement 1).

To obtain direct evidence that optogenetic illumination in our behavioral setup activates sensory neurons, we used electrophysiology. We made extracellular recordings of the dorsal organ of individual larvae expressing CsChrimson in specific olfactory receptor neurons, and recorded the responses to red light activation pulses of 0.2, 0.5 and 1 second of the same intensity used in the behavioral experiments. We found that optogenetic activation of the ORN expressing Or45a reliably and reproducibly induced spike trains during exposure to red light (Fig 1C). Similar results were obtained using larvae expressing CsChrimson in the ORN expressing Or42a (Fig 1D). These results confirm direct correspondence between ON/OFF pulses of CsChrimson activation and induced spiking in single sensory neurons.

To map the input-output relationships with optogenetic interrogation of chemosensory neurons, we used reverse-correlation methods viewing the whole animal as a transducer. We subjected larvae to random patterns of optogenetic stimulation, and collected the statistics of all behavioral responses exhibited by the freely moving larvae. We used the simplest white process for reverse-correlation, a Bernoulli process where we assigned -1 for lights OFF and +1 for lights ON, and calculated the mean stimulus history that preceded each run to turn or turn to run transition (Fig 1E, F). These event-triggered stimulus histories represent how the animal uses optogenetic activation patterns of specific neurons to regulate each motor state transition and are proportional to the linear filter components of $f_{r\to t}$ and $f_{t\to r}$ (see **Materials and Methods** **and** **Supplemental Methods**).

Linear filters of repellant and attractive responses

When freely crawling larvae encounter increasing chemoattractant concentrations during runs, they decrease the likelihood of initiating a turn. When they encounter increasing chemoattractant concentrations during the head sweep of a turn, they increase the likelihood of starting a new run. The Or42a receptor is activated by a number of volatile chemoattractants including ethyl butyrate and ethyl acetate (7, 8, 18). Genetically modified animals in which the *Or42a* expressing ORN is the only functional olfactory receptor neuron are capable of climbing olfactory gradients towards these attractants. These observations strongly suggest that the *Or42a* expressing ORN mediates attractant responses. To test our system, we subjected *Or42a>CsChrimson* larvae to random optogenetic stimulation. We found that run-to-turn transitions coincided with a decrease in the probability of optogenetic activation (Fig 2A, left), whereas turn-to-run transitions coincided with an increase (Fig 2A, right). These patterns are consistent with an attractive response to Or42a activation. Importantly, the full shape of the event-triggered stimulus histories informs us about how the temporal optogenetic activation patterns of Or42a regulate each type of navigational movement. Methods that measure the tendency of larvae to aggregate near chemoattractants or net movement up chemoattractant gradients provide information about the overall tendency to navigate but not about the discrete decision-making processes that drive navigation.

Random optogenetic activation of all the ORNs via expression of *UAS-CsChrimson* with the *Orco* olfactory-receptor-coreceptor driver (previously called *Or83b*) mediated an attractive response similar to the one shown with the *Or42a* driver alone (Fig 1E,F). This is consistent with most ORNs in the *Drosophila* larva being thought to mediate attractant responses (7, 19). One exception is the *Or45a*-expressing ORN, which has recently been shown to mediate an aversive response in an optogenetic setup; larvae that express Channelrhodopsin in *Or45a*-expressing neurons will avoid an illuminated region of an agar plate (20). A role for the *Or45a*-expressing neurons in repellency is also consistent with the observation that they are the only ORNs that detect octyl acetate, a chemical repellant (7, 21). We sought the linear filters of this olfactory repellant response in our setup by quantifying the movements of *Or45a>CsChrimson* larvae subjected to random optogenetic stimulation (Fig 2B). Run-to-turn transitions in *Or45a>CsChrimson* larvae coincided with an increase in the probability of optogenetic illumination and turn-to-run transitions coincided with a decrease, consistent with repellant behavior.

For comparison, we calculated event-triggered stimulus histories using larvae heterozygous for UAS-CsChrimson and with the same genetic background as our Gal4 lines (w1118 x UAS-*CsChrimson*) subjected to random illumination (Fig 2C). These control larvae were raised in the same conditions and fed the same food as larvae used for all other experiments (**Materials and Methods**). These larvae showed no correlations between the probability of illumination and motor state transitions. Their motor state transitions were random and spontaneous.

In our setup, we flag turn-to-run transitions by the resumption of peristaltic forward movement and run-to-turn transitions as the onset of head sweeping behavior. However, the decision to finish a run may begin at an earlier point, when the animal first begins to slow down. We measured the crawling speeds of larvae before flagged run-to-turn transitions, and found that runs decelerate ~1s before the onset of head sweeping behavior (Fig 2A-C). For both repellant and attractants, an increase and decrease in the probability of optogenetic illumination, respectively, coincides with the beginning of run deceleration (Fig 2A,B). The average deceleration time was 1s for all experiments conducted in this study (Student's t-test, $p<0.01$).

Linear-Nonlinear models of behavior

A satisfactory model of navigation should be able to predict behavioral responses to various stimulus waveforms. We asked whether we could use our measurements of event-triggered stimulus histories to build such a model. A simple and widely used formalism is the linear-nonlinear (LN) model. In LN models, the linear filter component is proportional to our measurement of the event-triggered stimulus history (15). First, the stimulus waveform is passed through this linear filter to make an initial prediction of the behavioral response. Linear estimates have common problems, such as taking negative values and failing to account for saturation. To correct these problems, the linear prediction is then scaled with a static nonlinear function. This static nonlinearity can be calculated by comparing a linear prediction with experimental measurements.

We used larvae with CsChrimson in *Or45a* expressing neurons to test an LN model in predicting behavior. We calculated the static nonlinearity for both run-to-turn and turn-to-run transitions by comparing linear predictions obtained with the event-triggered stimulus histories shown in Fig 2B with experimental measurements (Fig 3A). Next, we implemented the linear filter and static nonlinearity in an LN model (Fig 3B) to predict the behavioral response of these larvae to different inputs, using step increases in optogenetic illumination as well as defined trains of pulses of different widths. We found remarkably good agreement in these predictions to both stimulus types (Fig 3C). We note that the LN prediction begins to fail to account for the turn-to-run transitions at long times following a step increase in optogenetic illumination. Turns typically last <4 seconds, which limits the length of stimulus history that can be used in a linear filter, which thus puts a ~4s upper bound on the length of stimulus response that can be predicted. Taken together, our results show that LN models governing stimulus-evoked transitions between motor states can be used to predict larval chemotaxis behavior with high accuracy (Fig. 3C). The LN model was also successful in predicting the behavior of *Or42a*-expressing neurons and other chemosensory neurons (Fig 3-figure supplement 1; Fig 3-figure supplement 2; detailed calculations are in **Supplemental Methods**).

Distinct temporal dynamics in optogenetically-induced chemotactic behavior

The dynamics of behavioral responses are shaped by the linear filter component of LN models while the static nonlinearity only provides saturation and instantaneous scaling. To test if optogenetic activation of different chemosensory neurons could produce behavioral responses with distinct dynamics we undertook a search for different linear filters measured by event-triggered stimulus histories using reverse-correlation.

The Gr21a receptor senses carbon dioxide, a powerful *Drosophila* repellant (9, 22). We measured the event-triggered stimulus histories of *Gr21a>CsChrimson* larvae subjected to random optogenetic stimulation. We found that run-to-turn transitions coincided with an increase in the probability of optogenetic illumination from baseline, whereas turn-to-run transitions coincided with a decrease (Fig 4A). These patterns are consistent with a repellant response. However, the linear filter associated with Gr21a for run-to-turn transition revealed important differences in shape and timing of stimulus history as compared with the filter for Or45a. The run-to-turn transition in both cases was preceded by a positive lobe in the probability of optogenetic activation lasting ~2s. This positive lobe was itself preceded by a pronounced negative lobe lasting ~1.5s for Gr21a but not for Or45a.

How do differences in the shape and timing of linear filters translate into behavioral responses with different dynamics? To explore this question, we compared the prediction and experimental measurement of stepwise activation of *Or45a* and *Gr21a* expressing neurons (Fig 4B). Biphasic linear filters – such as that associated with Gr21a and also seen in other sensory systems like the *E. coli* chemotactic response – contribute to adaptation following transient stimulation (23). A step increase in stimulation with repellants will cause a transient increase in the probability of run-to-turn transition. We predicted and confirmed differences in the adaptive return to baseline behavior for Gr21a and Or45a. The probability of run-to-turn transition returns to baseline faster in the case of Gr21a. Since each point represents a distribution of binary values (larvae transitioning from running to turning and larvae not transitioning), we used a z-test to identify regions where $P(r \rightarrow t)$ is significantly higher than baseline with $p<0.05$. We found that $P(r \rightarrow t)$ of Gr21a larvae reach values significantly higher than baseline at least 0.5s earlier than Or45a larvae. In addition, Or45a larvae stay at elevated values of $P(r \rightarrow t)$ for at least 0.75s longer than Gr21a larvae (Fig 4-figure supplement 1A).

We also asked whether differences in behavioral dynamics caused by different linear filters might be found in attractant responses. Gr2a is expressed in the A1 and A2 GRNs of the dorsal organ as well as in two unidentified neurons in the terminal organ (12). The role of the Gr2a receptor is not known, but it is part of the subfamily of Gr68a which has been identified as a pheromone receptor in the adult fly (24). We calculated the event-triggered stimulus histories of *Gr2a>CsChrimson* larvae, and found that run-to-turn transitions coincided with a decrease in optogenetic activation, consistent with an attractant response (Fig 4C). Interestingly, the linear filter associated with Gr2a was distinct from that of Or42a. In

Or42a>CsChrimson, the run-to-turn transition was preceded by a single negative lobe lasting ~2s. In *Gr2a>CsChrimson* larvae, the negative lobe was itself preceded by a positive lobe. As we did for repellants (Fig 4B), we asked whether the response dynamics to step decrease in optogenetic stimulation were distinct. We predicted and confirmed differences in behavioral dynamics. The most noticeable feature is that Or42a larvae reach different steady states of $P(r \rightarrow t)$ for lights ON or OFF; this creates differences in step response dynamics. We conducted a z-test to identify regions where $P(r \rightarrow t)$ is significantly higher than baseline with $p<0.05$. Since the steady state $P(r \rightarrow t)$ for Or42a larvae is different for lights ON and lights OFF, we conducted the z-test with both values (Fig 4-figure supplement 1B). Because Or42a larvae start at a lower $P(r \rightarrow t)$, they take at least 1.75s longer than Gr2a larvae for $P(r \rightarrow t)$ to become significantly higher than the lights OFF steady-state $P(r \rightarrow t)$. Comparison with the steady state $P(r \rightarrow t)$ for lights ON confirms that the steady state $P(r \rightarrow t)$ for lights OFF is significantly higher with $p<0.05$ (Fig 4-figure supplement 1B).

We note that unlike the linear filters for run-to-turn transitions, the linear filters for turn-to-run transitions showed a similar shape for all Gal4 drivers that we used in this study. These filters only showed some variation in amplitude (Figs 1, 2, 4, 5).

Navigational responses from bitter-sensing GRNs

The molecular and cellular organization of the chemosensory system of the *Drosophila* larva is numerically simple. The 21 olfactory receptor neurons (ORNs) contained in the larval dorsal organ (DO) together express 25 members of the Or family of odorant receptors and the Orco coreceptor (11, 25). In contrast, 10 gustatory receptor neurons (GRNs) distributed in the dorsal organ and terminal organ – named A1, A2, B1, B2, and C1-C6 – together express 28 members of the Gr family of gustatory receptors. Whereas most ORNs express a single Or, GRNs can express multiple Grs and each Gr can be expressed in multiple GRNs (12). Thus, using larvae expressing CsChrimson under the control of different *Grx*-Gal4 drivers enabled us to assess the contribution of selected GRNs to behavior.

The C1 neuron expresses 17 receptors, some of which are found in other neurons (e.g., Gr32a which is also found in B2) and some of which are specific to C1 (e.g., Gr9a). Most Grs are thought to respond to repulsive bitter compounds because they express the bitter markers Gr33a and Gr66a (12), suggesting that C1 is a broadly tuned mediator of repellant responses. Consistent with this hypothesis, optogenetic activation of C1 with random stimuli using *Gr9a>CsChrimson* larvae evoked a weak repellant response where the run-to-turn transition coincided with a slight increase in the probability of optogenetic illumination (Fig. 5A) (this response was significantly different than the control with $p<0.05$, see Fig5-Supplementary Fig1A). Optogenetic activation of C1 together with B2 using *Gr32a>CsChrimson* larvae evoked a much stronger repellant response (Fig. 5B). Optogenetic activation of specifically the B2 neuron using *Gr10>CsChrimson* larvae evoked a repellant response (Fig. 5C) Optogenetic activation of C1 together with C4 using *Gr39a.b>CsChrimson* larvae generated a strong repellant response (Fig. 5D). One

possibility is that co-activation of narrowly tuned GRNs that express fewer Grs potentiates the repellant response of the broadly tuned C1 GRN; however, this interpretation should be taken with caution since different Gal4 drivers may induce different spiking rates upon optogenetic activation with CsChrimson.

We found that optogenetic activation of the C2 neuron alone using *Gr94a>CsChrimson* larvae evoked a weak attractive response (Fig 5E) (this response was significantly different than the control with $p<0.05$, see Fig5- Supplementary Fig1B). This is surprising because the C2 neuron also expresses the bitter receptors Gr33a and Gr66a, which should drive repellant responses, although these receptors are also found in other neurons. One possibility is that the attractant response driven by C2 is inverted when additional gustatory neurons are recruited. This hypothesis is supported by our observation that co-activation of C1 and C2 using *Gr39a.a>CsChrimson* larvae exhibited a much stronger repellant response than activation of C1 alone (Fig. 5F). Co-activation of C1, C2, and C4 using *Gr59d>CsChrimson* larvae also exhibited a strong repellant response (Fig. 5G). The strongest repellant response was observed by co-activating C1-C4, B1, and B2 using *Gr66a>CsChrimson* larvae (Fig. 5H).

Discussion

A fundamental step towards understanding how animal navigation is encoded in neural circuits is the development of a quantitative framework that accurately describes behavioral dynamics. To take this step with the *Drosophila* larva, we combined optogenetics with high-resolution behavioral analysis and reverse-correlation techniques to build linear-nonlinear models that provide an accurate estimate of the decision-making processes that guide navigation during optogenetically induced chemotaxis.

Linear-nonlinear models separate time-dependencies and instantaneous scaling into two modules, the linear filter and static nonlinearity, respectively. We find that the LN model is capable of accounting for diverse dynamics across attractant and repellant responses in both the gustatory and olfactory systems. For example, LN models accurately predicted the differences in response speed and adaptation when different GRNs and ORNs were activated. One reason for the diversity of dynamics is that the *Drosophila* larva chemosensory system, in addition to encoding attractant and repellant responses, is also capable of shaping the dynamics of behavioral responses in ecologically important ways. For example, the priorities given to specific chemicals encountered in the environment might not only be measured in terms of their relative degrees of attraction or repulsion, but also in the speed of the behavioral response that they trigger or the speed of adaptation. We note that some of the observed differences in behavioral dynamics might be caused by using different transgenic lines and different Gal4 drivers with different potencies. It would thus be useful to confirm the differences in behavioral dynamics that are suggested by our optogenetic manipulations with direct stimulation of each GRN and ORN and quantitative behavioral analysis in defined environments using cell-specific odorants and tastants.

Navigational dynamics evoked by specific sets of gustatory neurons have remained elusive because of the lack of chemicals that are specific to individual GRNs. Our reverse-correlation analysis using optogenetic activation with CsChrimson allowed us to determine not only the valence (attraction or repulsion) of navigation mediated by different combinations of GRNs, but also the dynamics of the evoked behavior. Although little is known about the circuits downstream of the GRNs, our analysis of sensorimotor transformations serves as a reference to determine how these circuits organize navigational decision-making.

Although chemotactic navigation behavior involves just two motor states (running and turning), it is possible, in principle, to extend reverse-correlation analysis to a larger number of possible behavioral states. Vogelstein *et* al presented recently a study where they used optogenetic pulses to trigger different subsets of neurons throughout the larval brain (26, 27). They identified 29 statistically different behavioral states, likely because they were able to interrogate circuits for a much wider variety of larval behaviors than navigation. It would be useful to apply reverse-correlation methods such as ours to examine transitions between this rich set of behavioral states to identify how specific neurons mediate a broader range of behavioral decisions than navigation up or down stimulus gradients.

The wiring diagram of the *Drosophila* larva nervous system is likely to be the next whole animal connectome that will be reconstructed (28). Powerful genetic tools are making it possible to target specific neurons throughout the *Drosophila* nervous system with cellular resolution (27). The new availability of powerful optogenetic tools for activating and inactivating neurons, particularly red-shifted molecules that are outside the spectrum of *Drosophila* vision, are making it possible to pinpoint the role of specific neurons in overall behavior (13, 29). An essential step in building whole nervous system models of behavior that incorporate wiring and dynamics is computational modeling. Bringing together computational modeling of behavior with new tools for behavioral and physiological analysis, such as those described here, should open the door to a thorough understanding of behavioral circuits from sensory input to motor output in the small but surprisingly sophisticated nervous system of the *Drosophila* larva.

Acknowledgments

We thank Vivek Jayaraman for sharing fly stocks, Ni Ji for comments on the manuscript, and Vivek Venkatachalam, Christopher Tabone, Renaud Bastien, Matthew Berck and Jess Kanwal for useful discussions. This work was supported by grants from the NIH to JC and to ADTS (1P01GM103770 and 8DP1GM105383-05).

Materials and Methods

Drosophila stocks

All larvae were raised in the dark at 22 °C and fed yeast with 0.5 mM all-*trans*-retinal (ATR). All *GrX-Gal4* lines were previously described (30). The *UAS-CsChrimson* flies were a gift of Vivek Jayaraman. Other lines were provided by the Bloomington Stock Center: *Or42a-Gal4* (BL#9970), *Or45a-Gal4* (BL#9975), *Orco-Gal4* (BL#23909), *Gr21a-Gal4* (BL#23890), *Gr66a-Gal4* (BL#28801), and *w1118* (BL#5905).

Behavioral assays

Male *Gal4* flies were crossed to *UAS-CsChrimson* virgins in small cages (Genesee Scientific) where eggs were laid on grape juice plates. Larvae were thoroughly washed in water, and late second instar larvae were selected under a dissecting microscope. For spatial navigation assays, groups of 20-30 larvae were placed in the center of a ~5 mm thick 22x22 cm agar (Fisher Scientific) plate and allowed to freely move for 20 minutes. Animals were recorded with a CCD Mightex camera with a long pass (740nm) infrared filter at 4Hz.

Light stimulation was produced with a custom built LED matrix assembled with SMD 5050 flexible LED strip lights of 12V DC and 625nm wavelength (LEDlightninghut.com) and controlled with an H bridge driver and custom code written for a LabJack U3 controller. Random light sequences were synchronized with the acquisition of images of the camera. Illumination was at 850nm wavelength with custom built LED bars. Technical considerations for assembly of the experimental setup are explained in the **Supplementary Methods**.

Electrophysiology

We followed previously described methods (11). In brief, action potentials of the olfactory receptor neurons (ORNs) were extracellularly recorded by placing a custom made tungsten recording electrode (with a piezo manipulator) through the cuticle into the dome of the dorsal organ of third instar larvae. The larva was placed on its ventrum on a metal rod and immobilized by wrapping Parafilm around the rod and the body, exposing only the very anterior part of the larva containing the domes of the dorsal organs. A reference electrode, a drawn out Borosilicate glass capillary filled with Ephrussi and Beadle solution, was previously inserted through the Parafilm into the larva's body. Light stimulation was generated with an LED at 627nm (Luxeonstar) driven by a buckpuck (LUXdrive LEDdynamics) and synchronized via a photocoupler relay (Toshiba TLP597A) with the data acquisition system (Syntech IDAC-4). The electrophysiological optogenetics experiments were conducted in a completely dark room, and the intensity of the light stimulus at the location of the larva's dorsal organ was set to 1.9 W/m^2.

Data analysis

The image stacks recorded were processed using MAGAT analyzer and analyzed using custom code written in MATLAB (9). To produce the random stimulus a Bernoulli process was used. This process is wide-sense stationary, produces independent binary values (Lights ON or OFF) at every instant, and its autocorrelation function is the Dirac delta function. The linear transformations for $r \rightarrow t$ and $t \rightarrow r$ transitions were estimated by the event-triggered averages multiplied by the mean $t \rightarrow r$ or $r \rightarrow t$ rates respectively (31, 32). The convolution of the filters with the stimulus was computed numerically without fitting any function to the filter. The number of larvae used in the experiments of each figure can be found in the respective legends. Details about the calculations, model construction and analysis of behavior can be found in the **Supplementary Methods**.

Figure Legends

Figure 1. Experimental method for reverse-correlation analysis using optogenetics.

(A) Larvae navigate by alternating between two basic motor states: runs and turns. The navigation strategy of the animal can be characterized by finding the mathematical functions, $f_{r\rightarrow t}$ and $f_{t\rightarrow r}$ that represent the stimulus dependence of transition rates.

(B) Schematic of experimental setup. Larvae crawl on a 22x22 cm agar plate. Dark-field illumination is provided by lateral infrared LED bars and animal movements are recorded with a CCD camera equipped with an infrared long pass filter. Optogenetic illumination is provided by a matrix of red 625nm LEDs from above.

(C) We made extracellular recordings in the olfactory organ of the *Drosophila* larvae. Here we show the rasters of the spikes induced by CsChrimson activation of the Or45a expressing ORN. We used 3 different pulse widths: 0.2, 0.5 and 1 second, all of them with the same intensity used for behavior experiments (1.9 W/m^2). The red bar in the top of each raster represents the period during which red lights were ON. Each vertical line in the raster represents one spike.

(D) Analogous to figure (C) we measured induced spiking of Or42a. The red bar in the top of each raster represents the period during which red lights were ON. Each vertical line in the raster represents one spike

(E) Mean stimulus history before each run-to-turn transition and (F) turn-to-run transition exhibited by *Orco>CsChrimson* larvae subjected to random ON/OFF optogenetic stimulation. The stimulus history for each motor state transition is aligned (dotted line) and averaged by assigning +1 to the LED ON state and -1 to the LED OFF state. Data represent mean (black line) +/- one SEM (grey shaded region) for 2018 transitions exhibited by 135 larvae. Twenty event-triggered stimulus histories are shown in the raster to illustrate the random binary stimulus pattern used in our experiments.

Figure 2. Olfactory receptor neurons evoked navigation strategy.

(A) Event-triggered stimulus histories for run-to-turn (left panel) and turn-to-run (right panel) transitions exhibited by *Or42a>CsChrimson* larvae subjected to random optogenetic stimulation as described in Fig. 1. Consistent with an attractive response, the likelihood of optogenetic activation falls before a run-to-turn transition and rises before a turn-to-run transition. In run-to-turn transitions, crawling speed begins to fall before the initiation of turning movements (green traces). The mean beginning of deceleration averaged over all animals is flagged by the red dot (+/- STD). The units of normalized speed are standard deviations away from the mean crawling speed during runs. Data represent mean (black line) +/- one SEM (grey shaded region) for 2752 transitions exhibited by 124 larvae.

(B) Event-triggered stimulus histories exhibited by *Or45a>CsChrimson* larvae. Consistent with a repulsive response, the likelihood of optogenetic activation increases before a run-to-turn transition and decreases before a turn-to-run transition. Data represent mean (black line) +/- one SEM (grey shaded region) for 3313 transitions exhibited by 119 larvae. The mean beginning of deceleration averaged over all animals is flagged by the red dot (+/- STD).

(C) Control larvae event-triggered averages. Event-triggered averages of control larvae were uncorrelated with red light illumination patterns. Data represent mean (black line) +/- one SEM (grey shaded region) for 4677 transitions exhibited by 121 larvae. The mean beginning of deceleration averaged over all animals is flagged by the red dot (+/- STD).

Figure 3. Linear-Nonlinear models of behavior.

(A) Estimating the static nonlinear function for run-to-turn and turn-to-run transitions exhibited by *Or45a>CsChrimson* larvae. Linear prediction using the event-triggered stimulus histories from Fig. 2B were compared with the experimental measurements that generated the stimulus histories. The static nonlinearity for the run-to-turn transition is fitted using least squares estimation of a sigmoidal function (R^2=0.8792). The static nonlinearity for the turn-to-run transition is fitted with a line (R^2=0.5041).

(B) Schematic representation of the linear-nonlinear model of navigation. Linear filters are convolved with the input signal and the result is scaled according to the static-nonlinear function fitted to estimate the probability rates for switching from one motor state to the other. (See **Supplementary Methods** for calculation details)

(C) LN model predictions (blue lines) of behavioral responses to step changes in optogenetic illumination (left panels) and defined random flicker (right panels). Predictions are made using the linear filter measured in Fig. 2B and the static nonlinearity measured in Fig. 3A. Experimental measurements to compare with prediction (black dots) represent data from N=120 for the step response prediction and N=240 larvae for the flicker response prediction.

Fig 4. Distinct navigation dynamics.

(A) Event-triggered stimulus histories exhibited by *Gr21a>CsChrimson* larvae. Linear filters of Gr21a neurons. Consistent with a repulsive response, the likelihood of optogenetic activation increases before a run-to-turn transition and decreases before a turn-to-run transition. Data represent mean (black line) +/- one SEM (grey shaded region) for 4680 transitions exhibited by 90 larvae. The mean beginning of deceleration averaged over all animals is flagged by the red dot (+/- STD).

(B) LN prediction and experimental measurements of different repellant responses to step changes in optogenetic illumination. Faster adaptation to baseline is observed in the case of the *Gr21a* expressing neurons than *Or45a*. Step responses were measured with 115 Gr21>CsChrimson larvae and 120 Or45a>CsChrimson larvae, each larva was subjected to 30 steps of optogenetic activation. (z-test substantiate significant difference in the dynamics of the cyan and black curves See Figure 4-figure supplement 1A)

(C) Event-triggered stimulus histories exhibited by *Gr2a>CsChrimson* larvae. Consistent with an attractive response, the likelihood of optogenetic activation decays before a run-to-turn transition and raises before a turn-to-run transition. Data represent mean (black line) +/- one SEM (grey shaded region) for 3672 transitions exhibited by 128 larvae. The mean beginning of deceleration averaged over all animals is flagged by the red dot (+/- STD).

(D) Linear prediction and experimental measurements of different attractant responses to step changes in optogenetic illumination. Faster responses and adaptation to baseline are observed in the case of the *Gr2a* than *Or42a*. Step responses were measured with 195 Gr2a>CsChrimson larvae and 117 Or42a>CsChrimson larvae, each larva was subjected to 30 steps of optogenetic activation. (z-test substantiate significant difference in the dynamics of the cyan and black curves See Figure 4-figure supplement 1B).

Fig 5. Reverse-correlation analysis of bitter-sensing GRNs.

Event-triggered stimulus histories exhibited by *GrX>CsChrimson* larvae using a set of GAL4 drivers that express in different subsets of GRNs. The cellular identities describing each expression pattern are taken

from Kwon et al. (2011). Each measurement represents 3270 to 4016 transitions taken from 87 to 134 larvae. Curves represent mean (black line) +/- one SEM (grey shaded region). The mean beginning of deceleration averaged over all animals is flagged by the red dot (+/- STD).

Figure supplements

Figure 1-figure supplement 1. Optogenetic activation of OK6-Gal4 motor neurons

To test if our experimental setup robustly activates CsChrimson, we expressed it in motor neurons using the *OK6-Gal4* driver (33) . Effective activation would result in most muscles of the larvae contracting simultaneously and not allowing larvae to crawl. Consistent with that, during illumination 100% of the 85 larvae tested stopped crawling during illumination and slowly recovered motility afterwards. The figure shows the mean speed (black line) +/- SEM (grey shaded area).

Figure 3-figure supplement 1. Linear-Nonlinear models of Gr21a and Gr10a

(A) Estimating the static nonlinear function for run-to-turn and turn-to-run transitions exhibited by *Gr21a>CsChrimson* larvae (left panels). Linear prediction using the event-triggered stimulus histories from Fig. 3A were compared with the experimental measurements that generated the stimulus histories. The static nonlinearity for the run-to-turn transition is fitted using least squares estimation of a sigmoidal function (R^2 = 0.9494). The static nonlinearity for the turn-to-run transition is fitted with a line (R^2= 0.5082).

LN model predictions (blue lines) and linear filter predictions (green lines) of behavioral responses to defined random flicker (right panels). Predictions are made using the linear filter measured in Fig. 3A and the static nonlinearity showed in the left panel. Experimental measurements to compare with prediction (black dots) represent data from N=156 larvae.

(B) Estimating the static nonlinear function for run-to-turn transitions exhibited by Gr10a>*CsChrimson* larvae (left panel). Linear prediction using the event-triggered stimulus histories from Fig. 5 were compared with the experimental measurements that generated the stimulus histories. The static nonlinearity for the run-to-turn transition is fitted using least squares estimation of a sigmoidal function with (R^2= 0.6221). At the resolution power employed in this study, the turn-to-run linear filter could not be distinguished from noise.

LN model predictions (blue lines) and linear filter predictions (green lines) of behavioral responses to defined random flicker (right panels). Predictions are made using the linear filter measured in Fig. 5 and the static nonlinearity showed in the left panel. Experimental measurements to compare with prediction (black dots) represent data from N=183 larvae.

Figure 3-figure supplement 2. Linear-Nonlinear models of Or42a and Gr2a

(A) Estimating the static nonlinear function for run-to-turn and turn-to-run transitions exhibited by Or42a>*CsChrimson* larvae (left panels). Linear prediction using the event-triggered stimulus histories from Fig. 2A were compared with the experimental measurements that generated the stimulus histories. The static nonlinearity for the run-to-turn transition is fitted using least squares estimation of a sigmoidal function with (R^2= 0.7617). The static nonlinearity for the turn-to-run transition is fitted with a sigmoid with (R^2= 0.625).

LN model predictions (blue lines) and linear filter predictions (green lines) of behavioral responses to defined random flicker (right panels). Predictions are made using the linear filter measured in Fig. 2A and

the static nonlinearity showed in the left panel. Experimental measurements to compare with prediction (black dots) represent data from N=207 larvae.

(B) Estimating the static nonlinear function for run-to-turn transitions exhibited by Gr2a>CsChrimson larvae (left panel). Linear prediction using the event-triggered stimulus histories from Fig. 4C were compared with the experimental measurements that generated the stimulus histories. The static nonlinearity for the run-to-turn transition is fitted using least squares estimation of a sigmoidal function with (R^2= 0.6752). LN model predictions (blue lines) and linear filter predictions (green lines) of behavioral responses to a step decrease (right panels). Predictions are made using the linear filter measured in Fig. 4C and the static nonlinearity showed in the left panel. Experimental measurements to compare with prediction (black dots) represent data from N=195 larvae.

Figure 4-figure supplement 1. Statistical analysis of behavioral dynamics

Each dot shown in Fig 4B,D is a probability but is also the mean of the distribution of larvae undergoing a run to turn transition if we consider each larvae undergoing this transition as 1 and larvae not undergoing this transition as 0. Then we have a distribution for each point in the cyan and black curves shown; each of those distributions can be compared with the distribution before the light stimulus is presented. Since we have sufficient data such that np >= 5 and n(1-p) >= 5 in all cases (n is the number of samples and p is the probability of undergoing a transition) we conducted a z-test to compare the distribution at each time point after opotgenetic stimulation with the baseline distribution. We show the p-values for each point in the case of Gr21a and Or45a in (A). All the p-values lower than 0.05 are shown, we note that Gr21a larvae become significantly different than their baseline behavior 0.5s before than Or45a larvae; in addition, Or45a larvae stay at values different from their baseline behavior for at least 0.75s longer than Gr21a larvae.

In the case of Or42a and Gr2a we conducted the same analysis (B middle) and obtained that Gr2a behavior becomes significantly different than baseline at least 1.75s before Or42a. However, in the case of Or42a, adaptation is only partial: Or42a larvae reach steady-state values of P(r->t) at different levels when red lights are ON or when red lights are OFF; because of that we also computed the z-test between Or42a after lights are turn OFF as compared to the distribution at the steady-state condition with lights ON. With this consideration we obtained a very small difference between Gr2a and Or42a rising time (B bottom). As observed, the distribution of Or42a larvae stayed at values significantly higher than the value of P(r->t) with lights ON.

Figure 5-figure supplement 1. Statistical analysis of Gr9a and Gr94a triggered average

The triggered averages of Gr9a and Gr94a showed very weak response. Because of this, we tested whether their observed behavior is significantly different than the control. Each point of the triggered averages is a distribution; thus we compared the distributions of each point with the corresponding one in the control with a t-test. In the case of Gr9a, it was only significantly different than the control for 0.75s of the 2s prior to the transition (panel A, bottom; the bottommost plot is a zoomed version of the middle plot). We obtained that Gr94a is significantly different than the control with p<0.05 1.75s before the transition (panel B, bottom).

Figure 5-figure supplement 2. Normalized speed of Gr lines

The normalized speed of each Gr line is shown. Normalized speed is computed using standard score. In all cases, the slowdown initiation happens 1s prior to the transition (t-test p<0.01). Red dots flag the slowdown initiation mean location (average of when the individual tracks start slowing down (changing the derivative of speed to negative) and the red bar is 2 standard deviations. The grey shaded regions near

526 the normalized speed value represent the SEM, in some cases is difficult to see because of the large
527 number of samples used: Each measurement represents 3270 to 4016 transitions taken from 87 to 134
528 larvae.

References

1. Mast SO (1938) Factors involved in the process of orientation of lower organisms in light. *Biological Reviews* 13(2):186–224.

2. Loeb J (1918) *The mechanistic conception of life: biological essays* (J.B. Lippincott and Company, Philadelphia, USA).

3. Saalfeld S, Fetter R, Cardona A, Tomancak P (2012) Elastic volume reconstruction from series of ultra-thin microscopy sections. *Nature Methods* 9(7):717–720.

4. Luo L, et al. (2010) Navigational decision making in Drosophila thermotaxis. *J Neurosci* 30(12):4261–4272.

5. Gomez-Marin A, Stephens GJ, Louis M (2011) Active sampling and decision making in Drosophila chemotaxis. *Nat Commun* 2:441.

6. Gomez-Marin A, Louis M (2012) Active sensation during orientation behavior in the Drosophila larva: more sense than luck. *Curr Opin Neurobiol* 22(2):208–215.

7. Kreher SA, Mathew D, Kim J, Carlson JR (2008) Translation of sensory input into behavioral output via an olfactory system. *Neuron* 59(1):110–124.

8. Louis M, Huber T, Benton R, Sakmar TP, Vosshall LB (2007) Bilateral olfactory sensory input enhances chemotaxis behavior. *Nat Neurosci* 11(2):187–199.

9. Gershow M, et al. (2012) Controlling airborne cues to study small animal navigation. *Nature Methods* 9(3):290–296.

10. Vosshall LB, Stocker RF (2007) Molecular Architecture of Smell and Taste in Drosophila. *Annu Rev Neurosci* 30(1):505–533.

11. Kreher SA, Kwon JY, Carlson JR (2005) The molecular basis of odor coding in the Drosophila larva. *Neuron* 46(3):445–456.

12. Kwon JY, Dahanukar A, Weiss LA, Carlson JR (2011) Molecular and cellular organization of the taste system in the Drosophila larva. *J Neurosci* 31(43):15300–15309.

13. Klapoetke NC, et al. (2014) Independent optical excitation of distinct neural populations. *Nature Methods* 11(3):338–346.

14. Ringach D, Shapley R (2004) Reverse correlation in neurophysiology. *Cognitive Science* 28:147–166.

15. Geffen MN, Broome BM, Laurent G, Meister M (2009) Neural Encoding of Rapidly Fluctuating Odors. *Neuron* 61(4):570–586.

16. Brand AH, Perrimon N (1993) Targeted gene expression as a means of altering cell fates and generating dominant phenotypes. *Development* 118(2):401–415.

17. Keene AC, Sprecher SG (2012) Seeing the light: photobehavior in fruit fly larvae. *Trends Neurosci* 35(2):104–110.

18. Asahina K, Louis M, Piccinotti S, Vosshall LB (2009) A circuit supporting concentration-invariant odor perception in Drosophila. *J Biol* 8(1):9.

19. Mathew D, et al. (2013) Functional diversity among sensory receptors in a Drosophila olfactory circuit. *Proc Natl Acad Sci USA* 110(23):E2134–43.

20. Bellmann D, et al. (2010) Optogenetically Induced Olfactory Stimulation in Drosophila Larvae Reveals the Neuronal Basis of Odor-Aversion behavior. *Front Behav Neurosci* 4:27.

21. Cobb M, Dannet F (1994) Multiple genetic control of acetate-induced olfactory responses in Drosophila melanogaster larvae. *Heredity (Edinb)* 73 (Pt 4):444–455.

22. Faucher C (2006) Behavioral responses of Drosophila to biogenic levels of carbon dioxide depend on life-stage, sex and olfactory context. *J Exp Biol* 209(14):2739–2748.

23. Block SM, Segall JE, Berg HC (1982) Impulse responses in bacterial chemotaxis. *Cell* 31(1):215–226.

24. Bray S, Amrein H (2003) A putative Drosophila pheromone receptor expressed in male-specific taste neurons is required for efficient courtship. *Neuron* 39(6):1019–1029.

25. Fishilevich E, et al. (2005) Chemotaxis behavior mediated by single larval olfactory neurons in Drosophila. *Curr Biol* 15(23):2086–2096.

26. Vogelstein JT, et al. (2014) Discovery of Brainwide Neural-Behavioral Maps via Multiscale Unsupervised Structure Learning. *Science* 344(6182):386–392.

27. Pfeiffer BD, et al. (2008) Tools for neuroanatomy and neurogenetics in Drosophila. *Proc Natl Acad Sci USA* 105(28):9715–9720.

28. Cardona A, et al. (2010) An integrated micro- and macroarchitectural analysis of the Drosophila brain by computer-assisted serial section electron microscopy. *PLoS Biol* 8(10).

29. Chuong AS, et al. (2014) Noninvasive optical inhibition with a red-shifted microbial rhodopsin. *Nat Neurosci* 17(8):1123–1129.

30. Weiss LA, Dahanukar A, Kwon JY, Banerjee D, Carlson JR (2011) The molecular and cellular basis of bitter taste in Drosophila. *Neuron* 69(2):258–272.

31. Sakai HM (1992) White-noise analysis in neurophysiology. *Physiol Rev* 72(2):491–505.

32. Dayan P, Abbott LF (2001) *Theoretical Neuroscience* (MIT Press, Cambridge, MA USA).

33. Sanyal S (2009) Genomic mapping and expression patterns of C380, OK6 and D42 enhancer trap lines in the larval nervous system of Drosophila. *Gene Expr Patterns* 9(5):371–380.

Figure 1

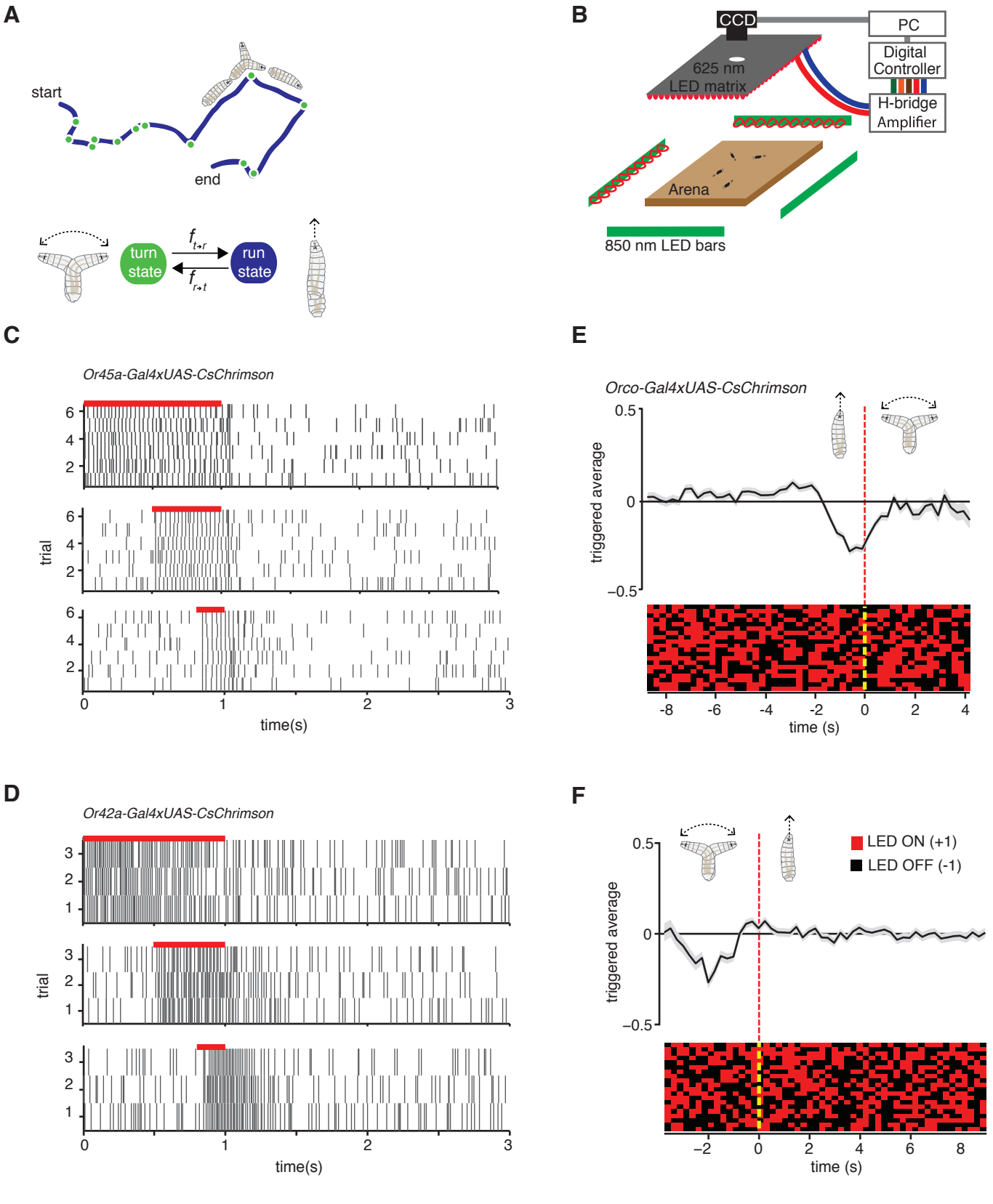
A
start
end
turn state
run state
B
CCD
PC
Digital Controller
625 nm LED matrix
H-bridge Amplifier
Arena
850 nm LED bars
C
Or45a-Gal4xUAS-CsChrimson
trial
time(s)
D
Or42a-Gal4xUAS-CsChrimson
trial
time(s)
E
Orco-Gal4xUAS-CsChrimson
triggered average
time (s)
F
LED ON (+1)
LED OFF (-1)
triggered average
time (s)

Figure 2

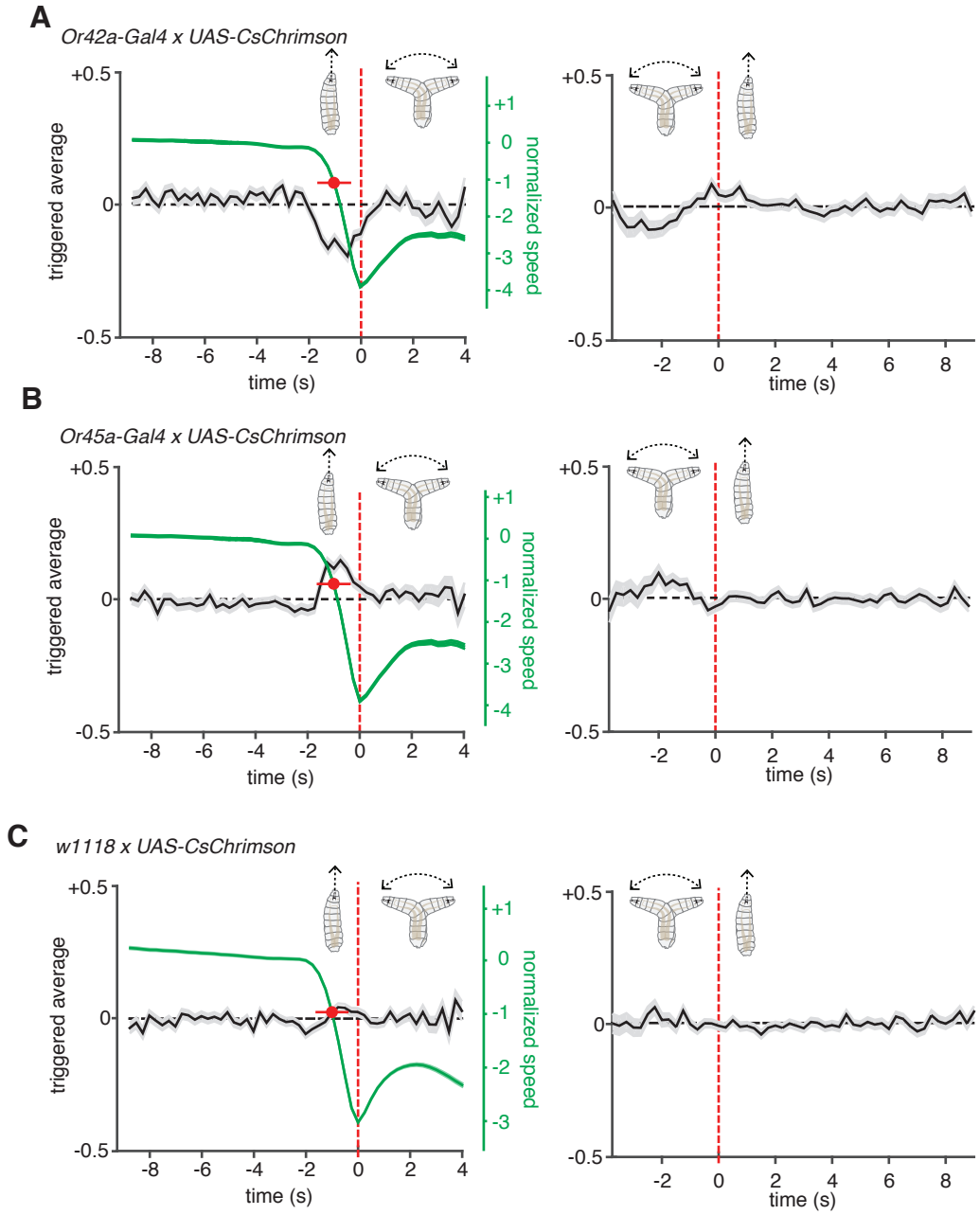
A
Or42a-Gal4 x UAS-CsChrimson
B
Or45a-Gal4 x UAS-CsChrimson
C
w1118 x UAS-CsChrimson
triggered average
normalized speed
time (s)
+0.5
0
-0.5
+1
-1
-2
-3
-4
-8
-6
-4
-2
2
4
6
8

Figure 3

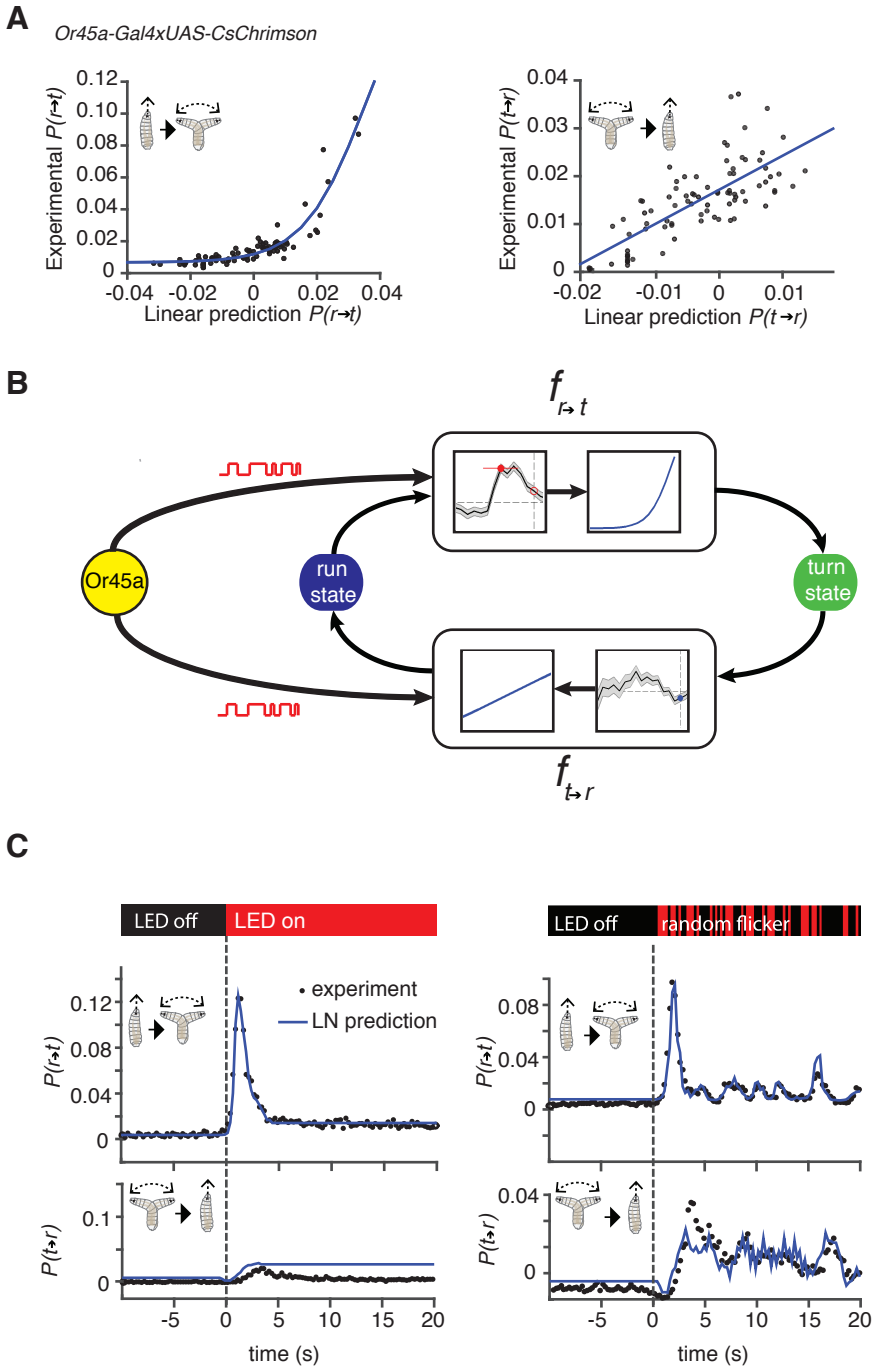
A
Or45a-Gal4xUAS-CsChrimson
Experimental P(r→t)
Linear prediction P(r→t)
Experimental P(t→r)
Linear prediction P(t→r)
B
Or45a
run state
turn state
C
LED off
LED on
random flicker
• experiment
LN prediction
P(r→t)
P(t→r)
time (s)

Figure 4

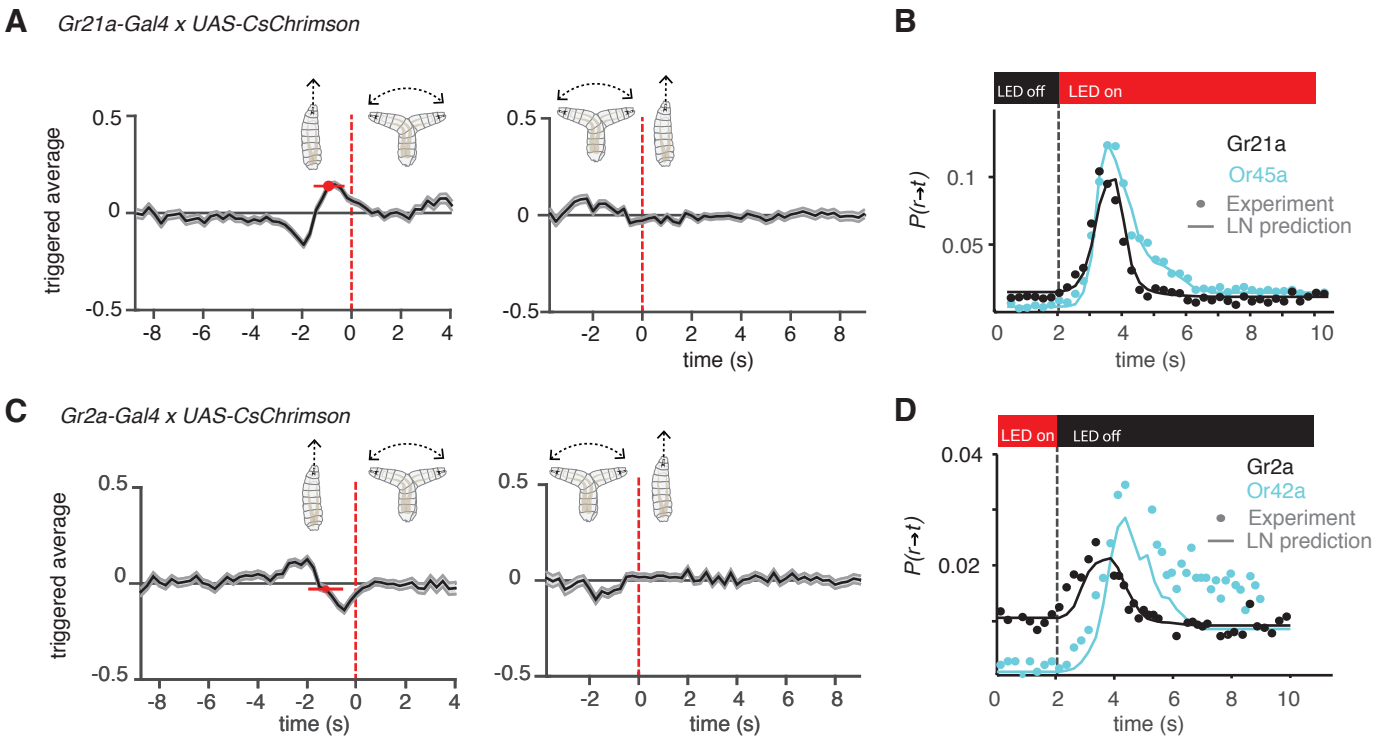
A
Gr21a-Gal4 x UAS-CsChrimson
triggered average
0.5
0
-0.5
-8 -6 -4 -2 0 2 4
-2 0 2 4 6 8
time (s)
B
LED off
LED on
Gr21a
Or45a
Experiment
LN prediction
P(r→t)
0.1
0.05
0 2 4 6 8 10
time (s)
C
Gr2a-Gal4 x UAS-CsChrimson
triggered average
0.5
0
-0.5
-8 -6 -4 -2 0 2 4
time (s)
-2 0 2 4 6 8
time (s)
D
LED on
LED off
Gr2a
Or42a
Experiment
LN prediction
P(r→t)
0.04
0.02
0 2 4 6 8 10
time (s)

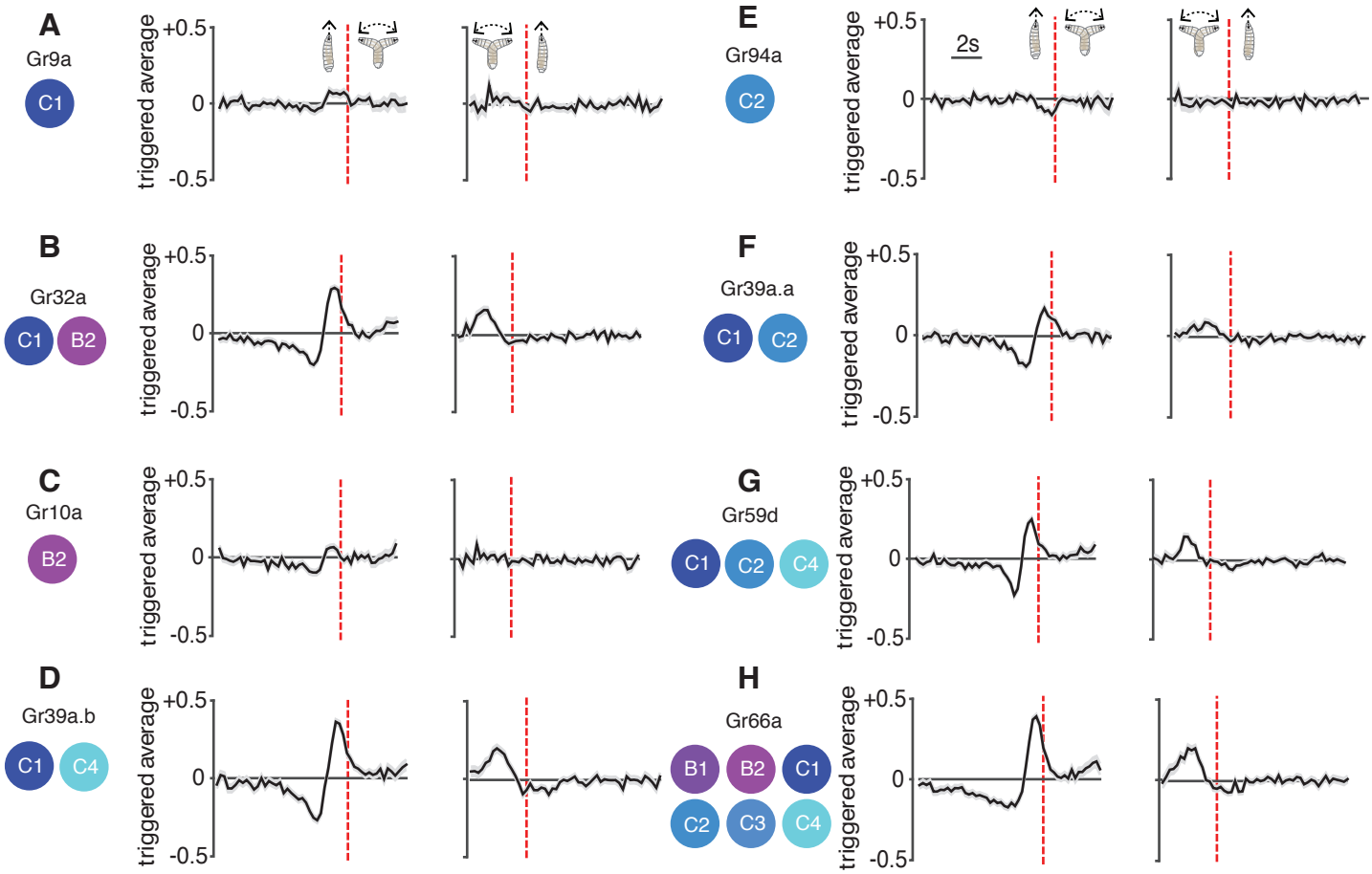
A
Gr9a
C1
triggered average
+0.5
0
-0.5
B
Gr32a
C1
B2
C
Gr10a
B2
D
Gr39a.b
C1
C4
E
Gr94a
C2
2s
F
Gr39a.a
C1
C2
G
Gr59d
C1
C2
C4
H
Gr66a
B1
B2
C1
C2
C3
C4

Figure 1-figure supplement 1

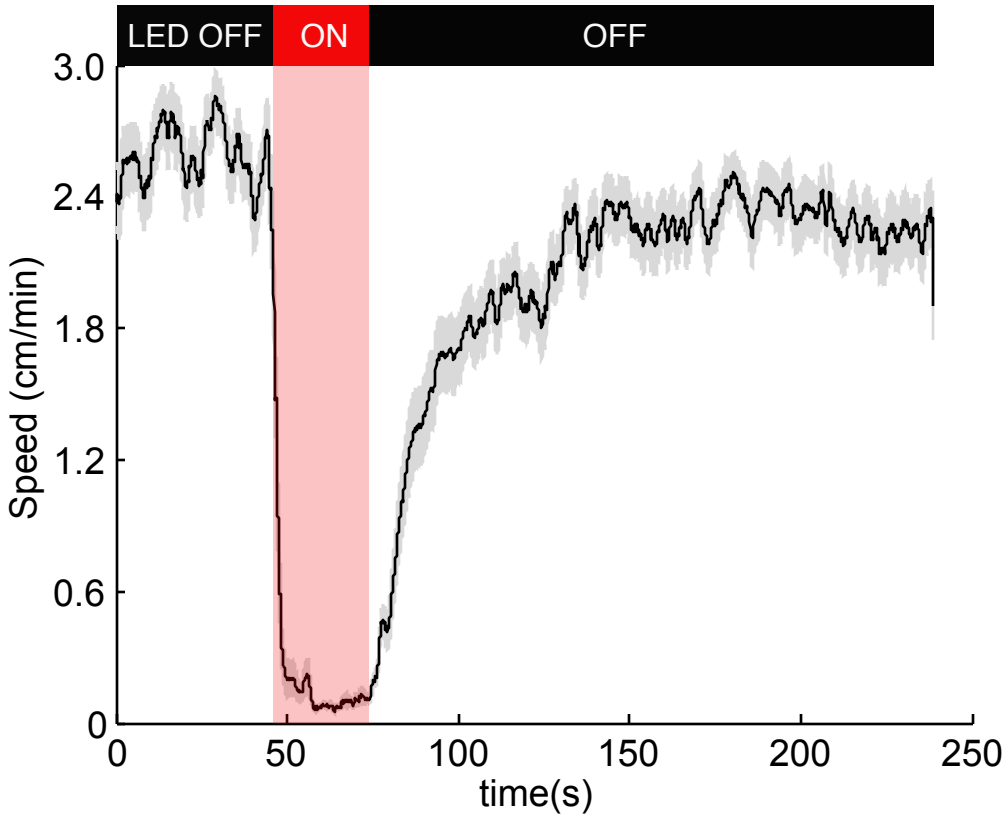

Figure 3-figure supplement 1

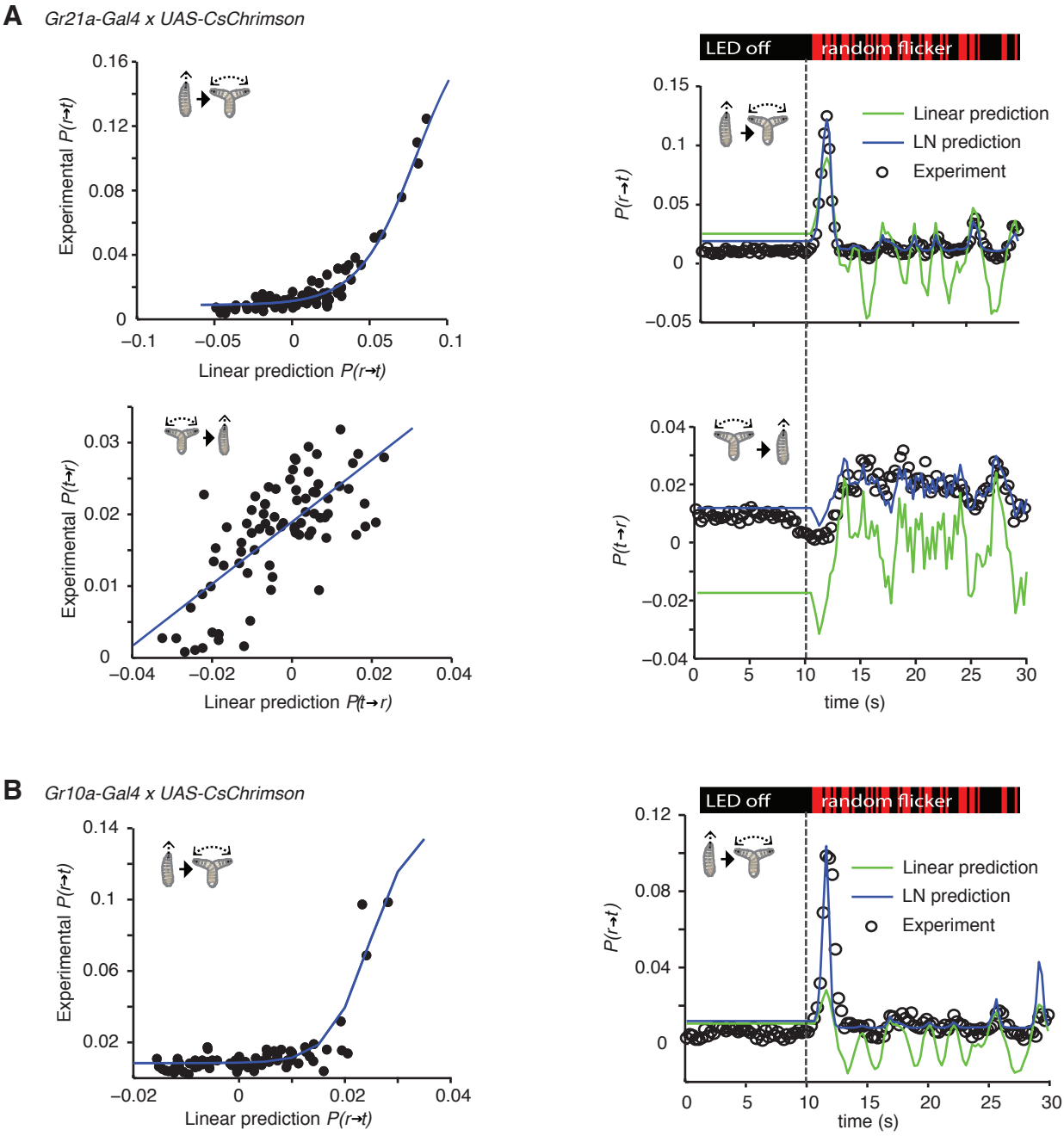

Figure 3-figure supplement 2

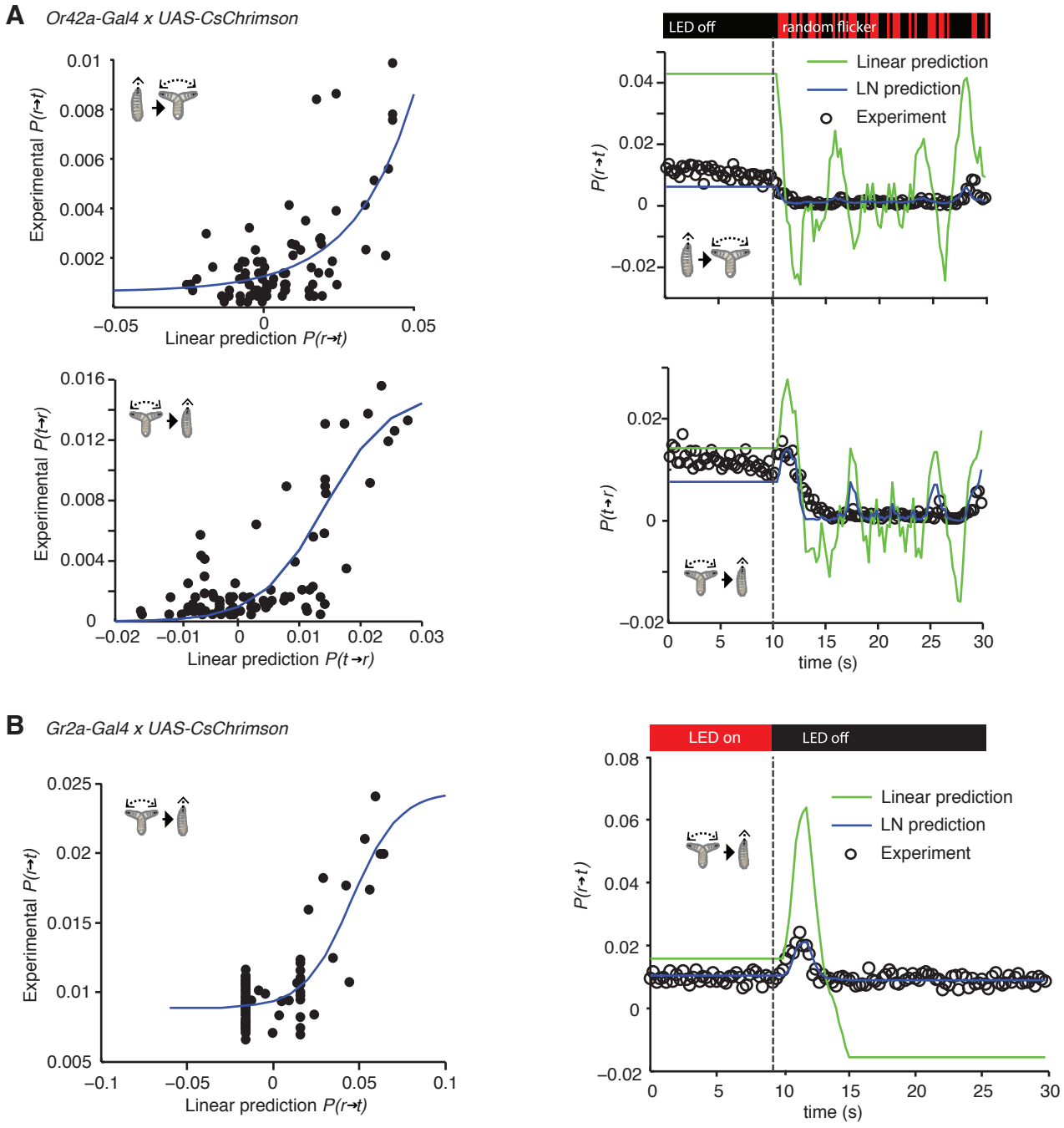

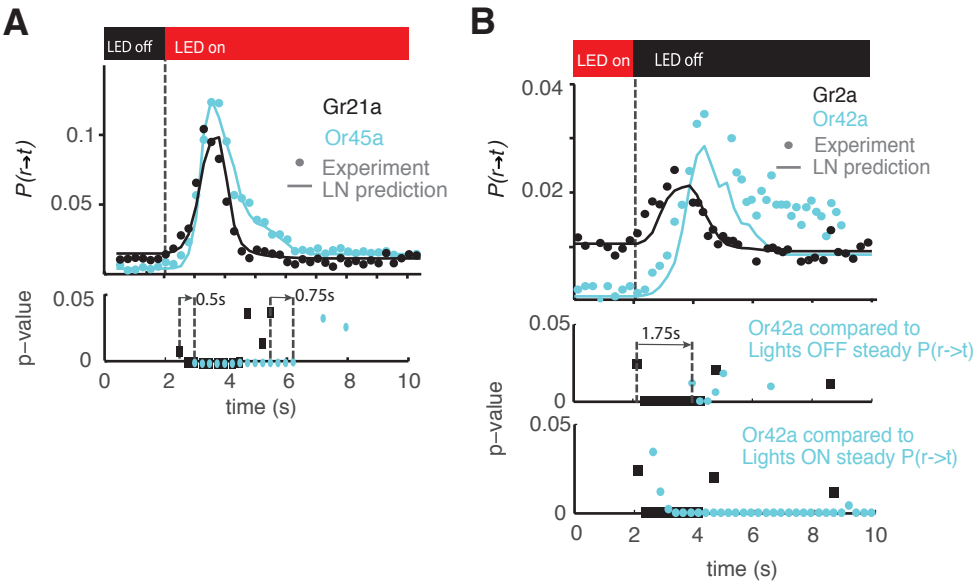
A
LED off
LED on
Gr21a
Or45a
Experiment
LN prediction
P(r→t)
0.1
0.05
p–value
0.05
0
0.5s
0.75s
0
2
4
6
8
10
time (s)
B
LED on
LED off
0.04
0.02
Gr2a
Or42a
Experiment
LN prediction
P(r→t)
0.05
0
1.75s
Or42a compared to
Lights OFF steady P(r->t)
p–value
0.05
0
Or42a compared to
Lights ON steady P(r->t)
0
2
4
6
8
10
time (s)

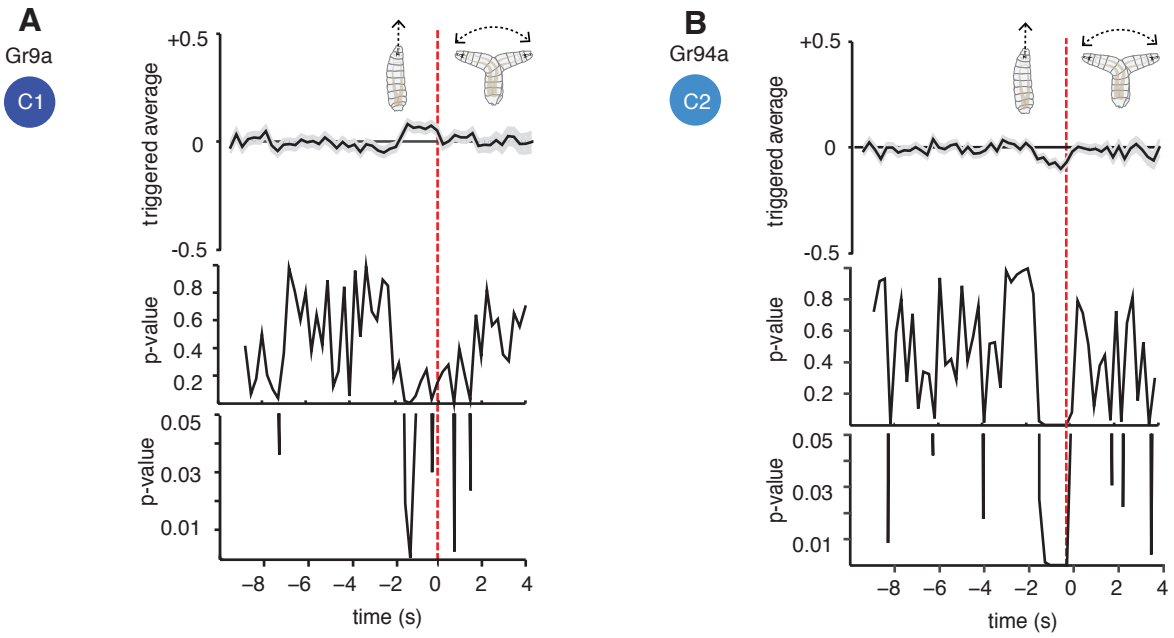
A
Gr9a
C1
triggered average
+0.5
0
-0.5
p-value
0.8
0.6
0.4
0.2
p-value
0.05
0.03
0.01
−8
−6
−4
−2
0
2
4
time (s)
B
Gr94a
C2
triggered average
+0.5
0
-0.5
p-value
0.8
0.6
0.4
0.2
p-value
0.05
0.03
0.01
−8
−6
−4
−2
0
2
4
time (s)

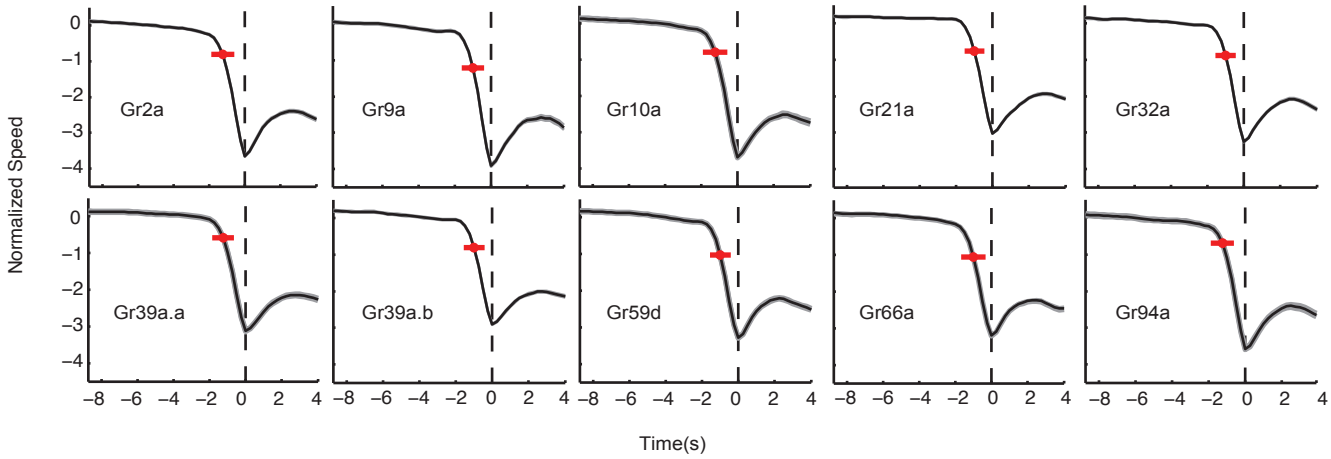
Normalized Speed
Gr2a
Gr9a
Gr10a
Gr21a
Gr32a
Gr39a.a
Gr39a.b
Gr59d
Gr66a
Gr94a
0
−1
−2
−3
−4
−8 −6 −4 −2 0 2 4
Time(s)